NORSAR

ROYAL NORWEGIAN COUNCIL FOR SCIENTIFIC AND INDUSTRIAL RESEARCH

Scientific Report No. 2 - 81/82

SEMIANNUAL TECHNICAL SUMMARY

1 October 1981—31 March 1982

By
Jørgen Torstveit (ed.)

Kjeller, July 1982

Sponsored by
Advanced Research Projects Agency
ARPA Order No. 2551

VI.3 Seismic array configuration optimization

The seismological concept of arrays emerged from the nuclear test ban negotiations in Geneva in 1958 when the need for improved capability to study weak seismic events was clearly recognized. Over the years many kinds of array systems have been installed in many countries, but LASA and NORSAR remained the unique ones; unique in terms of their sizes (apertures of the order of 200 and 100 km, and number of instruments once 588 and 198, respectively), and because dedicated data centers were made an integral part of these arrays.

In Norway a miniarray termed NORESS (NORSAR Experimental Small Subarray) has recently been installed within the NORSAR array itself and is shown in Fig. VI.3.1. The motivation for this undertaking is to provide data for optimum design of a complete array system for surveillance of events at regional distances. This is the research topic dealt with in this section.

Signal and noise structure

An essential aspect of the array design is a priori assumptions regarding the statistical structure of signal and noise. Generally speaking, the array response when 'steered at' the signal, should be small at wavenumbers characteristic of the noise. Intersensor spacings would then correspond to maximum correlation for the signal and a minimum for the noise. A common assumption has been that of equal signals and uncorrelated noise beyond a critical space lag, and for sufficiently large intersensor spacing the array design criteria are trivially met. However, observations usually contradict these assumptions, and our optimization procedure will be based on actually observed signal and noise correlations using NORESS recordings.

Signal correlations

A major objective of our work was to derive an optimum layout for detecting events at regional distances, so signal correlations were measured for phases identified as Pg, Pn and Lg for the 5 events listed in Table VI.3.1,

all within 12° of NORESS. A record section of Event 5 is displayed in Fig. VI.3.2, signal correlations in Fig. VI.3.3. We see that the Pg phase exhibits high correlation values for all frequency bands and sensor separations displayed. The Lg phase on the other hand correlates rather poorly in the higher frequency ranges. The results for the Pn phase show increasing correlation with frequency, which reflects a corresponding peak in the signal spectrum around 4 Hz.

Noise correlation

Selected noise records, including both summer and winter conditions, were subjected to correlation analysis, and the results obtained are also given in Fig. VI.3.3. The most notable feature here is that the correlation curves consistently have a negative minimum before tending to zero, which is rated significant. This observational fact, easily missed when noise similarity is expressed via the coherency measure, is consistent with a model of propagating noise, as demonstrated by Mykkeltveit et al (1982).

In Fig. VI.3.4 we show the theoretical correlation function for noise with a uniform wavenumber spectrum in the range $(2\pi)^{-1}$ to $5\cdot(2\pi)^{-1}$ c/km. This wavenumber range would be appropriate for typical Rayleigh wave phase velocities (3-4 km/s) in a frequency range roughly 0.6 to 3 Hz, or typical body wave phase velocities (above 6 km/s) at frequency above 1 Hz. The curve is reasonably close to the observed curve which is taken from Fig. VI.3.3 and testifies to the importance of propagating noise at the Rayleigh wave velocities, even at relatively high frequencies. This is in accord with the results of wavenumber analysis, although higher phase velocities typical of body waves are also observed.

The optimization procedure

Let signal to noise ratio gain by beamforming be expressed by

$$G^2 = \sum_{ij} w_i w_j c_{ij} / \sum_{ij} w_i w_j \rho_{ij} \qquad (1)$$

where c_{ij} is the signal correlation between sensors i and j, ρ_{ij} similarly describes the noise correlation and w_i are sensor weights. In the common beamforming practice at arrays, w_i=1. Then, since $c_{ii} = \rho_{ii} = 1$, equation (1) can be rewritten in the more common form:

$$G^2 = \frac{1+(N-1)\bar{c}}{1+(N-1)\bar{\rho}} \qquad (2)$$

where $\bar{c}$, $\bar{\rho}$ describe average signal and noise correlations for an N sensor array. Alternatively, it is possible to use weighted beamforming (e.g., Christoffersson and Husebye, 1974), and the optimum gain function for noise suppression is simply the reciprocal maximum likelihood estimate of noise power (c.f. Boverie and Gregg, 1971):

$$G'^2 = \sum_{ij} \rho_{ij}^{-1}$$

where ρ_{ij}^{-1} form the inverse correlation matrix of the noise. Our reasons for optimizing G rather than G' are that (i) G with unit weights reflects the common beamforming practice at arrays, (ii) G contains both noise and signal, (iii) G is more stable with respect to variations in the estimate of noise correlation.

The gain is a nonlinear function of the sensor coordinates, and for more than three sensors we obtained a maximum of G by applying a standard rapid descent method (Fletcher and Powell, 1963) to analytic approximations of the correlation functions in Fig. VI.3.3. As might be expected, the optimum configuration is strongly determined by the position of the noise correlation minimum, but for relatively poorly correlating signals like Lg, the slope of the signal correlation curves is also important. Since these features are frequency dependent (see Fig. VI.3.3), different optimum geometries will result for different frequency bands. A compromise is to optimize a combination of the gains in different frequency bands.

Figs. VI.3.5 and VI.3.6 show examples of the gain averaged over the 5 frequency bands of Fig. VI.3.3, where the optimization was done sequentially from 3 to 20 sensors. Whereas the gain for Lg is near the standard factor $\sqrt{N}$ (in amplitude), which results from the assumption of identical signals and uncorrelated noise, the gain for Pg is systematically higher.

Our final configuration with 20 sensors for Pg gives a gain 4 dB above $\sqrt{N}$. As demonstrated in Fig. VI.3.7, together with the gains in individual frequency bands. For example, in Fig. VI.3.7 we have included the optimum geometry for the frequency band 1.6-4.0 Hz, with clearly reduced intersensor spacings as compared to the averaged geometry for the 5 frequency bands. Corresponding results for Lg are given in Fig. VI.3.8; here the optimum geometry for frequency band 1.6-4.0 Hz has larger dimension than the averaged geometry.

Obviously, the optimum 3 sensor array should form an equilateral triangle, with intersensor spacing close to the noise correlation minimum. From Figs. VI.3.5 and VI.3.7 it is clear that for Pg the same optimum intersensor spacing dominates the array geometry for a larger number of sensors. An illustrative example is the optimum geometry for 20 sensors (Fig. VI.3.7), with two pairs of sensors near the center of the array. This is interpreted as indicating the importance of these positions, with a maximum number of other sensors at optimum distance. For Lg (Figs. VI.3.6 and VI.3.8), similar observations can be made with regard to number of sensors and array dimension, the principal difference being that, due to reduced signal correlations, intersensor spacings and array dimension are also reduced. More generally, the trade-off between the effect of increased number of sensors and increased array dimension should be considered for limiting the final number of sensors in the regional array. Another important point is that the array performance inevitably would depend on phase type and frequency, but 'worst case' events can be considerably improved by flexible weighting schemes.

Although the main scope of our study has been array design for surveillance of regional events, the methodology applied is not limited to this task. For example, our array concept is also the likely basic subarray unit in a large aperture ('teleseismic') array, in which case the 'optimum' main/side lobe strategy for deployment of subarray units as once used for LASA and NORSAR would be adequate. A more comprehensive presentation of the work synthesized above is given by Mykkeltveit et al (1982).

S. Mykkeltveit
K. Åstebøl
D.J. Doornbos
E.S. Husebye

References

Boverie, B. and W.D. Gregg (1971): A signal detectability approach to optimizatin of the geometry of distributed aperture (array) receivers. I.E.E.E. Trans. Ant. Prop. AP-19, 22-30.

Christoffersson, A. and E.S. Husebye (1974): Least squares signal estimation techniques in analysis of seismic array recorded P-waves. Geophys. J.R. astr. Soc. 38, 525-552.

Fletcher, R. and M. Powell (1963): A rapidly convergent descent method for minimization. Comput. J. 6, 163-168.

Mykkeltveit, S., K. Åstebøl, D.J. Doornbos and E.S. Husebye (1982): Seismic array configuration optimization. Manuscript submitted for publication.

Date	Origin time	Location		Local Magnitude
06 Nov 1980	14.53.02	59.5°N	10.7°E	2.1
25 Nov 1980	02.39.49	58.4°N	13.7°E	2.4
29 Nov 1980	20.42.16	51.2°N	18.5°E	3.5
26 Feb 1981	17.43.53	60.3°N	15.9°E	2.1
01 Mar 1981	05.08.16	62.8°N	6.2°E	2.7

Table VI.3.1

Local events used in this study.

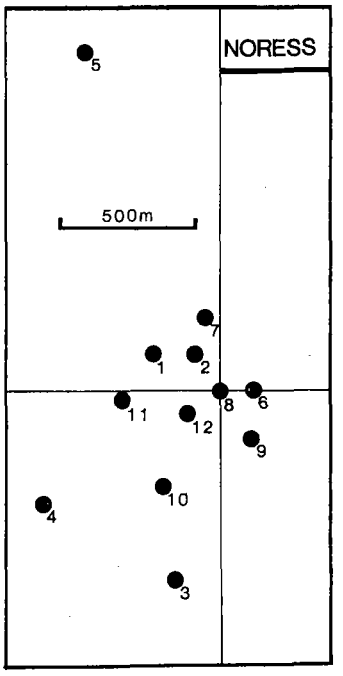

Fig. VI.3.1 Geometry of the 12-element NORESS array. All sensors are equipped with 4.75 Hz antialiasing lowpass filters.

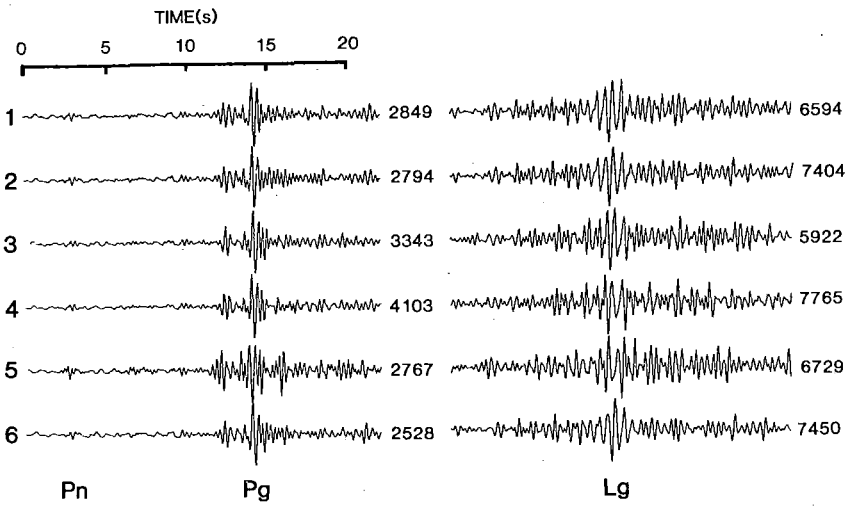

Fig. VI.3.2 NORESS records (channels 1-6 in Fig. VI.3.1) for event 5 in Table VI.3.1. For each phase, correlation measurements are made from 2 sec of data around the phase maximum. All traces are normalized, numbers to the right give scaling factors. The gap between Pg and Lg is 29 sec.

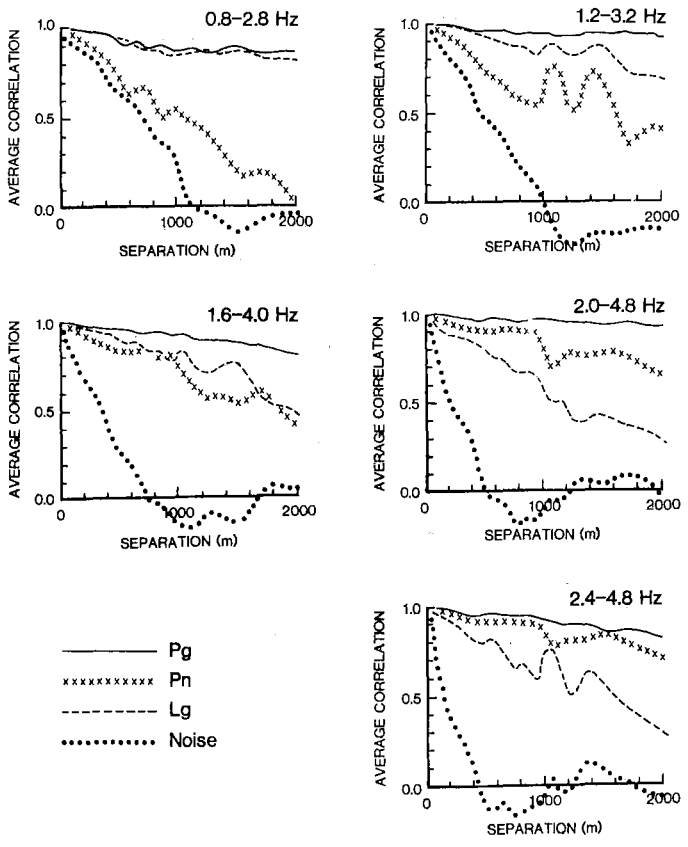

Fig. VI.3.3 Correlation vs distance for Pg, Pn, Lg and noise at NORESS for the five frequency ranges indicated. Each curve is based on measurements from 66 combinations of sensor pairs.

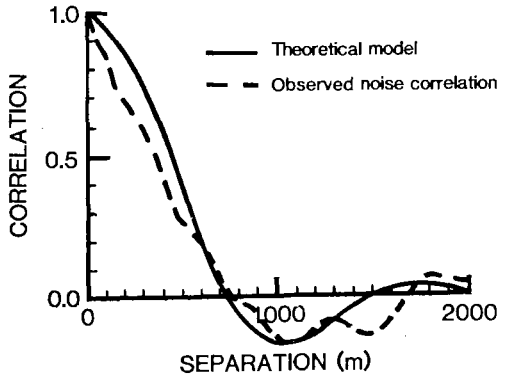

Fig. VI.3.4 Theoretical correlation function for noise with a uniform wavenumber spectrum in the range $(2\pi)^{-1}$ to $5(2\pi)^{-1}$ c/km. The observed noise correlation function (dashed line) is reproduced from Fig. Vi.3.3 (frequency range 1.6-4.0 Hz).

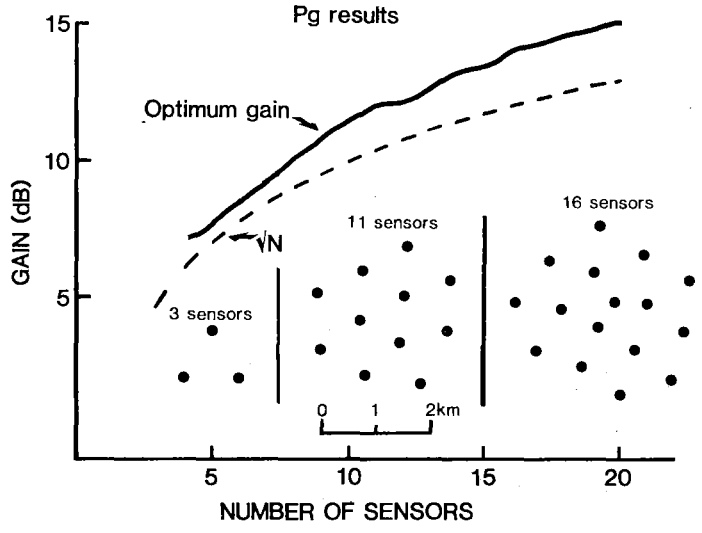

Fig. VI.3.5 Gain for the Pg phase as a function of number of sensors for geometries derived from our optimization procedure. The starting geometry for 3 sensors along with resulting geometries for 11 and 16 sensors are shown. The gain is an average over the 5 frequency bands in Fig. VI.3.3.

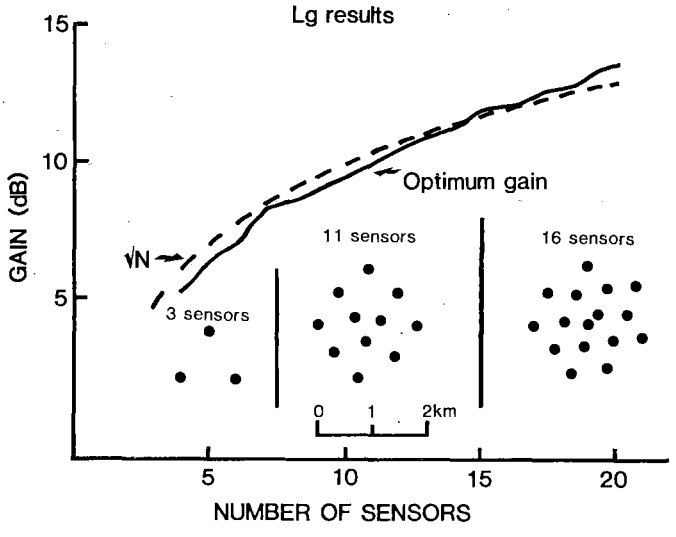

Fig. VI.3.6 Same as Fig. VI.3.5, but for the Lg phase.

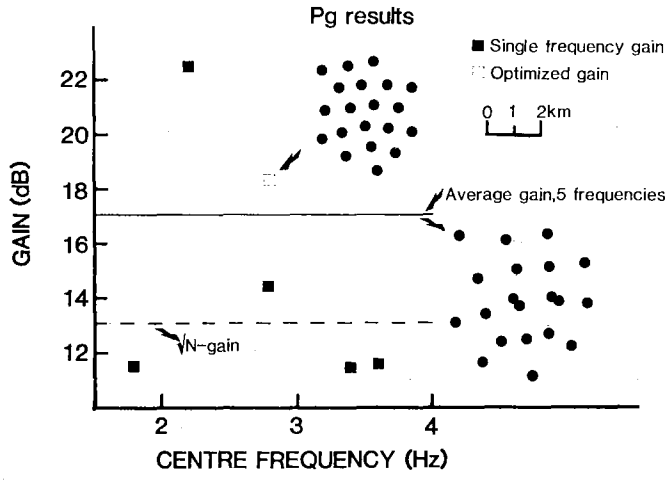

Fig. VI.3.7 Pg gains for an optimized 20-element array. The lower right geometry is optimum when the gain function is expressed as the sum of 5 individual gain functions for the frequency bands shown in Fig. VI.3.3. This geometry gives different gain for each band, as indicated by the 'single frequency gains'. The geometry derived from a 'mulitple' gain function is different from that based on a single frequency band. This is demonstrated by reoptimizing the lower right configuration for the frequency band centered at 2.8 Hz resulting in a net gain of 4 dB and a new geometry as shown. The exceptionally large gain for the frequency band centered at 2.2 Hz reflects the pronounced negative noise correlation observed here (see Fig. VI.3.3).

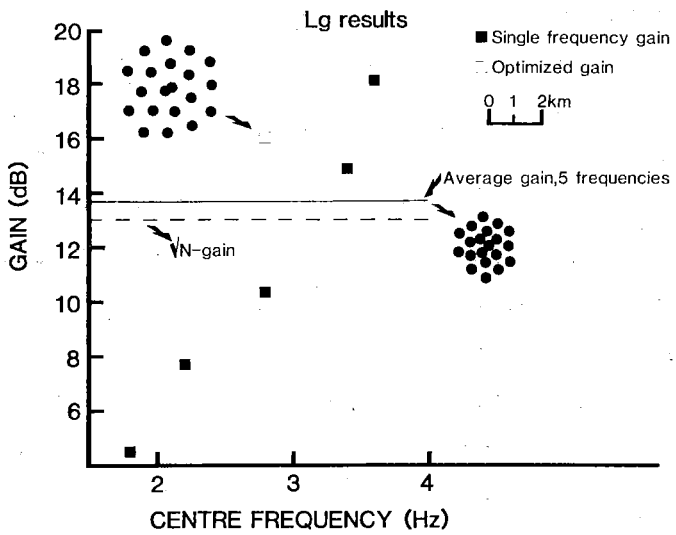

Fig. VI.3.8 Lg gains for an optimized 20-element array. The geometry to the right is optimum when the gain function is expressed as the sum of 5 individual gain functions in the frequency bands given in Fig. VI.3.3. This geometry gives different gains for each band, as indicated by the 'single frequency gains'. The optimum geometry derived from a 'multiple' gain function is different from that based on a single frequency band. This is demonstrated by reoptimizing the lower right configuration for the frequency band centered at 2.8 resulting in a net gain of nearly 6 dB and a new geometry as shown. The higher frequency ranges are seen to dominate the 'average' geometry.